Fire Safety Journal 142 (2024) 104037

Contents lists available at ScienceDirect

Fire Safety Journal

journal homepage: www.elsevier.com/locate/firesaf

An approach for the improved measurement of pyrolysis products

Jonathan Reep [a,*], Jose L. Torero [b], Rory M. Hadden [a]

[a] The University of Edinburgh, School of Engineering, Scotland, UK
[b] University College London, Faculty of Engineering Science, England, UK

ARTICLE INFO

Keywords:
Pyrolysis
Toxicity
Effluent
Speciation
Emissions
Mass spectrometry
Fire chemistry
Smoke
PMMA
FPA
FT-IR
MMA

ABSTRACT

The composition of a fuel and the combustion environment are factors that impact pyrolysis processes. The pyrolysis of a natural polymer, timber, and the synthetic polymers, polymethylmethacrylate (PMMA) and polystyrene (PS), was performed at a constant mass loss rate (MLR) using a feedback control loop utilising the Fire Propagation Apparatus (FPA) under inert and oxidative environments. The controlled MLR (2 g s^{-1} m^{-2}) enabled a representative means of monitoring emissions via a combination of spectroscopic techniques. Reported yields were calculated utilising adapted Fourier-transform infrared spectroscopy (FT-IR) data based upon the species detected via gas chromatography-mass spectrometry (GC-MS). The speciation offered by the GC-MS was used to adjust recorded FT-IR yields, facilitating an insight into the composition of pyrolysis emissions. The presence of molecular oxygen was not found to drastically influence the decomposition behaviours of the investigated synthetic polymers with the yields of primary monomers being relatively unaffected by the atmospheric environment. However, a difference was noted when using timber, as the generated char was visually different under the oxidative atmospheres. The presence of char oxidation was confirmed as a lower applied heat flux was required to sustain the desired mass loss rate. We conclude that the proposed combined analytical approach shows great potential for tracking and quantifying effluent emissions.

1. Introduction

Pyrolysis processes underpin most fire problems. An improved understanding of pyrolysis pathways will enable a better linking between solid and gas phase processes which is essential to understand phenomena such as flame spread and ignition [1]. Additionally, the analysis of pyrolysis products is key to the assessment of smoke, determining whether a material is likely to generate species of concern as it burns [2]. Thus, the development of methods to advance our understanding of pyrolysis processes facilitates advancements throughout the fire science field.

The factors that impact the variety and yield of volatile species being generated within fire effluent are inherently linked to the environmental conditions. Exposure to elevated temperatures initiates the decomposition of larger molecules, forming smaller (lower molecular weight) species. These pyrolysis processes repeatedly occur, breaking down the newly formed molecules into shorter and shorter chains. Eventually these small molecules volatise, becoming entrained in air, where they may form a flammable mixture leading to ignition or be entrained into the fire plume as 'smoke'.

If a flame and adequate ventilation are present, generated pyrolysis products can be oxidised, either partially or completely, to produce combustion products. If the flame is well-ventilated (i.e. the reaction mixture is lean and the chemical timescales are short compared to the mixing timescales), then products of complete combustion will be favoured. In this case the complete oxidation of pyrolysis products occurs, generating water vapour (H_2O) and carbon dioxide (CO_2). Under-ventilated conditions favour incomplete combustion reactions, increasing the relative yields of carbon monoxide (CO) and unburnt species [3]. During full-scale fires, these under-ventilated conditions typically arise when ventilation from openings (doors/windows) is insufficient to provide the oxygen (O_2) required to sustain complete combustion.

Identifying and quantifying the species being produced by pyrolysis is an essential aspect to understanding material flammability. Material flammability varies depending on environmental conditions, however, two critical factors always remain; the type of species being volatilised and importantly, the concentration. Knowing how these species are formed begins with an understanding of how a material decomposes. As pyrolysis is a time dependent process and is sensitive to external factors,

* Corresponding author.
E-mail addresses: j.reep@sms.ed.ac.uk (J. Reep), J.Torero@ucl.ac.uk (J.L. Torero).

https://doi.org/10.1016/j.firesaf.2023.104037
Received 8 June 2023; Received in revised form 4 October 2023; Accepted 21 October 2023
Available online 21 October 2023

the mass of a sample must be monitored in real-time [4]. Therefore, to understand the process of pyrolysis, the resultant gas-phase emissions, and the rate of pyrolysis, must be measured to facilitate the calculation of product yields.

1.1. Pyrolysis processes

When solid materials undergo pyrolysis, there are three different global pathways of interest: sublimation, melting and evaporation, and charring. In order to evaluate the efficacy of any measurement approach, it is necessary to test it across these different material behaviours. Synthetic polymers largely comprise of one or two monomers, in a repetitive structure. The lack of both crosslinking and monomer variation allows plausible predictions into decomposition kinetics and pathways, enabling effluent composition to be estimated. Some simple synthetic polymers decompose to produce their corresponding monomer units.

The synthetic polymer polymethylmethacrylate (PMMA) has been studied extensively. PMMA is known to undertake a multi-step thermal decomposition. Initially monomers are lost from the end of the polymer chain via the dominant process known as chain-end scission [5]. If the heat flux experienced by a sample increases, the chain may split at random intervals, random scission, producing a mixture of monomers and oligomers. A lower temperature environment will hinder this random scission, potentially generating a different ratio of pyrolytic species. A plausible mechanism for this process is outlined in Fig. 1.

Through the comparison of pyrolysis under oxidative and inert atmospheres, it has been reported that oxygen has a stabilising effect on PMMA [6]. Utilising thermogravimetric analysis (TGA), the peak mass loss rate (MLR) for solid PMMA samples was observed to shift by 50 K when exposed to highly oxygenated environments. Further studies have proposed that the radical intermediate in Fig. 1 is stabilised by molecular oxygen, producing an oxygen based radical with a greater thermal stability [5]. This enhanced thermal stability increases the resistance to thermal decomposition, thus supressing further chain scission.

Another simple synthetic polymer, polystyrene (PS), has been studied under both inert and oxidative atmospheres, decomposing predominantly via chain-end scission to produce a mixture of monomers, dimers and trimers [7]. Existing TGA data has shown that the activation energy required to trigger PS decomposition in air was 75 kJ mol^{-1} lower than a comparative case under an inert environment [8]. These findings suggested that oxygen had a destabilising effect on this synthetic polymer, potentially enabling an alternative decomposition pathway.

For charring natural polymers like timber, the precise composition of the effluent varies significantly, largely attributed to differences in molecular composition and the chain-stripping that occurs during char formation. A complex mixture of fatty acid methyl esters (FAMEs), polycyclic aromatic hydrocarbons (PAHs), cellulose- and lignin-derived products are produced as the cellulosic chains in timber cleave [9]. The species generated will also depend on physical factors such as grain and the presence of knots influencing the distribution and transport of intermediate species within the wood. It is likely that many different species at low concentrations will be formed during the pyrolysis of timber. Given the suspected variation in product yields, timber was selected as a good means of assessing the limitations of the speciation and potentially the sensitivity of our adopted analytical methodology.

1.2. Existing techniques

A variety of approaches have previously been utilised in an attempt to quantify product yields. One approach involves the use of thermogravimetric techniques coupled to gas chromatography–mass spectrometry (GC-MS). Although insightful, the small sample sizes and controlled temperature ramps are unrepresentative of the volatilisation observed during the heating of a material throughout a fire. During a fire, the low heating rates impose isothermal conditions within the sample, creating transport processes that TGA neglects. The use of these tools has enabled an insight into oxidative pyrolysis helping to shape the understanding of pyrolytic mechanisms, however scaling this up to samples of the sizes used in flammability testing or in real fires remains uncertain [10].

Since, pyrolysis occurs as the result of heat transfer into a sample. The rate of both the heat transfer into the sample and the resultant mass transfer of pyrolysis products out of the sample are dependent on the sample's physical and geometric properties. These gradients are not established in microscale techniques, like TGA, which are designed to operate isothermally.

Species either directly produced (monomers, dimers etc.) or diffused (oxygen) will be present across these temperature and hence concentration gradients throughout the sample, impacting the rate at which species are emitted from the sample's surface. Therefore, in-depth heat and mass transfer, in part, determine the mass loss rate of the sample, thus impact the composition of the pyrolysis products. To improve our understanding of pyrolysis products, the relationship between the burning rate and the composition of pyrolytic species needs to be understood. It is therefore plausible that differences in the composition of gaseous pyrolysis products exist between a microscale sample in the TGA and a bench-scale sample.

Another widely used approach to characterise pyrolysis products, with a focus on smoke toxicity, is the Steady State Tube (Purser) furnace. This apparatus allows characterisation of gaseous effluent, with the apparatus enabling the simulation of well-, and under-ventilated combustion conditions [11]. A standard experiment involves a sample being passed into a furnace at a set rate, under a controlled airflow, and the resultant effluent is analysed. However, such a technique cannot relate the monitored emissions to the way in which the sample is burning as real-time mass loss cannot be measured and observations of the combustion mode (flaming, smouldering) cannot be easily made. Furthermore, the timescales required to perform adequate sampling of pyrolysis products requires steady state conditions. These usually do not occur in systems in which a thermal environment is imposed on the material.

This study moves beyond existing microscale techniques, rather than linking a specific temperature or air flow to the formation of pyrolysis products, effluent is assessed as an ensemble; linking the generated species to controlled mass loss rates. This enables the net heat flux to the sample to be assumed to be constant. The steady state pyrolysis rate also allows sampling techniques to be employed over longer time periods, increasing the types of analysis that can be utilised. Additionally, if a consistent MLR is established, the effects of remaining environmental factors, specifically oxygen concentration, on the emissions can be

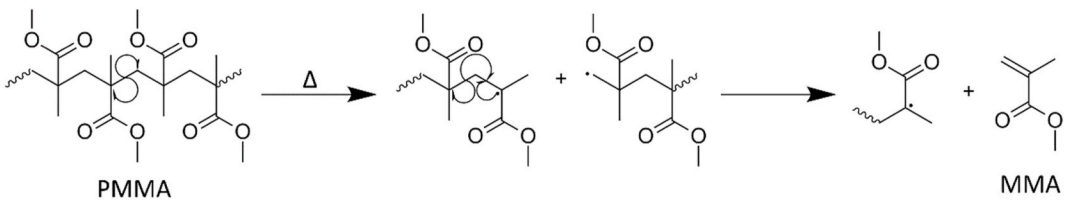

Fig. 1. A plausible mechanism for the thermal degradation of the polymer PMMA to form the monomer MMA. The initial cleavage generates two unstable radical species, enabling further decomposition [5].

assessed. If a constant MLR is observed, the impact of remaining factors including, surface temperature, oxygen composition and fuel type, can be studied in the context of the degradation pathways.

It is envisioned that flaming combustion may eventually be controlled in a similar way, enabling the methodology to facilitate an insight into combustion mechanics. The study also opens up the potential for large-scale work, enabling the investigation of emissions alongside the other flammability parameters as functions of oxygen concentration.

2. Methods and materials

2.1. Methodology

2.1.1. Constant mass loss rate

The Fire Propagation Apparatus (FPA) facilitates small-scale samples being subjected to an external heat flux whilst simultaneously enabling control over the surrounding oxygen concentration. To enable a constant MLR during pyrolysis, it was necessary to modify the standard FPA experimental procedure, E2058-19 [12]. A proportional integral derivative (PID) controller was created, enabling an automatic adjustment of the heat flux supplied to the sample by manipulating the voltage supplied to the lamps based on live mass measurements received from the inbuilt load cell [13].

PID controllers utilise a control loop to drive a system towards a target value, accounting for error, $e(t)$, which in this case was based on the difference between the calculated MLR and the desired MLR. Equation (1), where $u(t)$ represented a function of the error, was used to alter the voltage output sent to control the lamps for our PID controller.

$$u(t) = K_p e(t) + K_i \int_0^t e(t')dt' + K_d \frac{de(t)}{dt} \quad (1)$$

The output voltage sent to the lamps was the sum of each of the three terms in Equation (1). The three adjustable coefficients, K_p, K_i and K_d, summarised in Table 1, were individually adjusted to alter the means by which a target value was obtained.

Preliminary experimental work was conducted to optimise the coefficients K_p, K_i and K_d for each material. Over the course of forty iterations, the PID parameters were optimised to achieve the desired 2 g s^{-1} MLR. The effectiveness of the applied parameters was determined based on the time taken to reach a steady state, the extent of the oscillation whilst at this steady state and the range of voltages sent to the lamps.

Before each experiment, a heat flux gauge was used to calibrate the tungsten lamps. A predefined voltage ramp was sent to the lamps with the resultant heat flux being monitored over the course of this ramp. These values enabled the output voltages sent to the FPA lamps during experimental runs to be directly linked to the time varying heat flux values.

2.1.2. Sampling pyrolysis products

When investigating the composition of effluent generated during pyrolysis, two analytical techniques were deployed in tandem. In addition to the exhaust duct, two separate heated sampling lines (453 K) withdrew effluent. The heated sampling lines were situated above the quartz tube (150 mm) with one directed to a Fourier-transform infrared spectroscopy (FT-IR) cell (Gasmet, Vantaa, Finland) while the other passed through a condenser (dry ice/acetone, 195 K). Condensed effluent was collected to give a crude colourless liquid, products with a boiling point lower than 195 K could not be condensed.

The FT-IR analysis involved an IR beam being directed towards a gaseous sample drawn from the stream of pyrolysis products. The low energy beam was partially absorbed by molecules with a net dipole moment, triggering vibrational, rotational and translational transitions. Specific functional groups were shown to absorb at specific wavenumbers thus facilitating identification. The temporal measurements facilitated by the FT-IR enabled the effluent to be sampled every 4 s, however, only predetermined species could be monitored based on the predefined reference spectra. FT-IR analysis was conducted using a Gasmet DX4000 portable gas analyser. Produced IR spectra were analysed using the supplied software (Calcmet V2005.100, Tetmet Instruments Ltd., Vantaa Finland) alongside calibrated reference samples. Each spectrum was analysed across a spectral range (595–4240 cm^{-1}) with the resolution (8 cm^{-1}) achieved via a thermoelectrically cooled MCT detector coupled with an antireflection (ZnSe) beamsplitter. Gas samples were filtered (particulate, 2 μm) before entering the sample cell (0.4 L, 453 K). The path length (250 cm) proved adequate to maintain the sampling frequency.

The second sampling line passed effluent through a condenser ahead of ex-situ GC-MS analysis. After an experiment, collected condensed samples were volatilised and separated via GC, generating a total ion chromatogram (TIC) with a series of peaks. Each peak was analysed via MS fragmentation with the resultant fragment ions enabling explicit chemical identification. Quantification could be achieved via external standards, however data could only be collected over the whole run, not in real time (hence the requirement of constant pyrolysis rate). Therefore, the GC-MS was primarily used to confirm the identities of the species being detected via the FT-IR.

CH_2Cl_2 (3.25 mL) was added to the crude condensed effluent and the two layers were separated. The organic layer was extracted to give a colourless liquid. The resultant solution (~4 mL) was sealed in a Wheaton sample vial (12 mL) and taken for GC-MS analysis. GC-MS analysis was carried out using a Thermo Trace 1300 GC with an ISQ LT single quadrupole MS (Thermo Fisher Scientific, Massachusetts, USA), in splitless mode equipped with an AL 1310 liquid autosampler (Thermo Fisher Scientific, Massachusetts, USA), using a TraceGOLD TG-5 column (30 m × 0.25 mm × 0.25 μm), held at 308 K for 600 s before rising to 553 K at 273 K min^{-1}. A helium carrier gas was flowed at 0.8 mL min^{-1}. The MS had a 573 K ion source temperature and was operated in positive electron ionisation mode, scanning m/z 40–400.

2.1.3. Pyrolysis experiments

Samples of either PMMA (100 mm × 100 mm × 5 mm, 56.23 g), European whitewood (Norway spruce) (100 mm × 100 mm × 20 mm, 128.69 g) or polystyrene beads (contained in a circular foil dish, 100 mm in diameter, 5 mm in depth, 31.32 g) with the rear surface covered in foil, were individually placed onto a load cell situated within the housing of the FPA. A quartz tube (435 mm high, outer diameter 174 mm, inner diameter 164 mm) was placed over the sample.

After an initial ramp (0.02 kW m^{-2} s^{-1}, 60 s) the PID controller was initiated, controlling the voltage supplied to the four tungsten filament lamps and therefore the heat flux supplied to the specimen. The PID controller was set to enable a constant mass loss rate (2 g s^{-1}) over a set time period (800 s). An oxidiser flow of 100 L s^{-1} was maintained around the sample throughout each experiment, preventing a localised build-up of pyrolysis gases. The composition of this stream was 0%, 10%, or 21% O_2 with the balance being nitrogen. Each experiment was performed in triplicate, with sampling commencing after the mass loss rate had stabilised (200 s). This timeframe was chosen as it enabled all materials to reach the desired mass loss rate with minimal fluctuations. Fig. 2 shows a diagram of the complete experimental setup.

Table 1
The three parameters that can be adjusted in a PID controller [14].

Tuning Type	Applied Adjustment	Value
Proportional (K_p)	Relative to the difference between the current and target value.	2
Integral (K_i)	The sum of any error from the proportional term.	0.01
Derivative (K_d)	Slowing the rate at which the correction factor is applied.	8

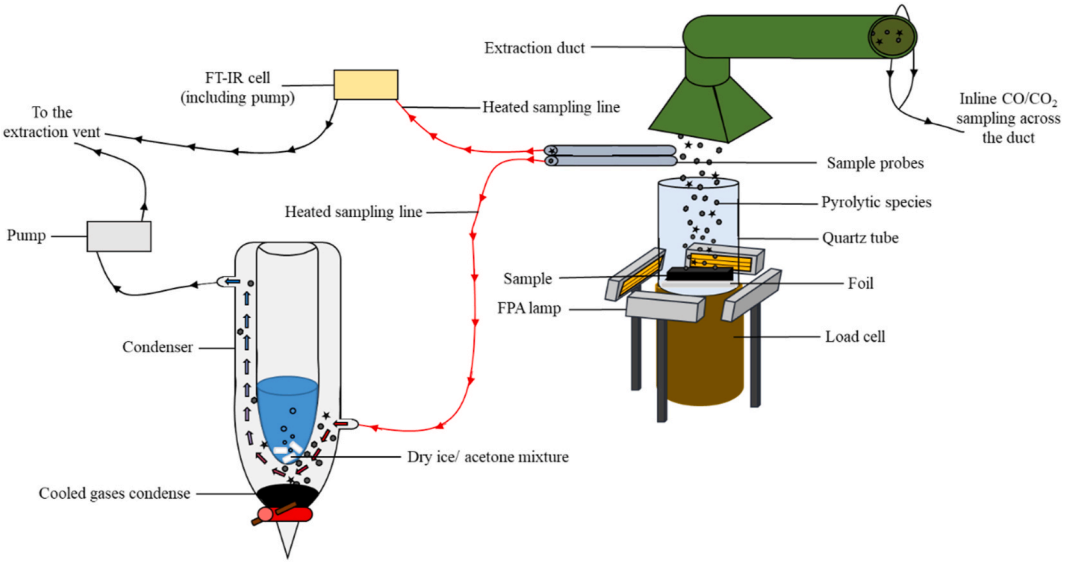

Fig. 2. The modified FPA setup. Effluent was generated from the pyrolysis of the sample placed inside the FPA. Two sample probes sampled generated effluent, passing it to the condenser or the FT-IR cell. Condensed effluent was subsequently extracted for GC-MS analysis.

2.2. Materials

The samples investigated in this study (PMMA, timber and polystyrene) were selected based upon their physical properties. The timber is a charring material, expected to produce a mixture of complex pyrolysis products including aliphatic and aromatic hydrocarbons, while the non-charring PMMA and melting PS were expected to generate their respective monomers; methyl methacrylate (MMA) and styrene.

Each of the samples were sourced commercially. The polystyrene arrived as white spherical pellets (~1 mm diameter), the timber as untreated boards and the PMMA as opaque black sheets, suggesting the presence of a colorant additive. The timber was a European whitewood (Norway spruce).

External standards were ordered to enable GC-MS areas to be quantified. Methyl methacrylate (MMA) (stabilised with hydroquinone monomethyl ether), styrene (stabilised with 4-tert-butylcatechol) and 2-methoxyphenol were obtained. All the standards used had purities of ≥99%. Standard solutions were formed using dichloromethane (DCM).

3. Results

3.1. Mass loss rate

As Fig. 3 details, the mass loss rate for each run stabilised, relative to initial fluctuations, at 2 ± 0.52 g s^{-1} m^{-2} after approximately 200 s had elapsed. The reported error was calculated from 220 s onwards for the polystyrene runs, as some samples were still in the process of melting. The fluctuation also disregarded the anomalous increase in mass loss rate for a single PMMA trial that peaked at 3.48 g s^{-1} m^{-2}. This peak is likely to have occurred due to sample mass falling from the load cell rather than an increased rate of pyrolysis.

The response to the PID controller for the PMMA and PS runs was much more varied than that of the timber. As the PMMA and PS underwent pyrolysis, bubbles formed on the sample's surface. These processes resulted in distinct periods of mass loss as the bubbles burst. These periods of discrete mass loss could not be managed by the PID controller resulting in fluctuations in the MLR.

When assessing the heat fluxes supplied by the FPA, approximately similar values were required to maintain the MLR across the different pyrolysis atmospheres for the synthetic polymers. However, the timber required a lower heat flux under oxidative environments to sustain the same mass loss rate. The applied heat flux, Fig. 4, remained below 40 kW m^{-2}, preventing flaming combustion from occurring [15]. The decreased heat flux, ~25 kW m^{-2}, required to sustain the same MLR under oxidative conditions has been attributed to the presence of char oxidation which contributed to mass loss in addition to the pyrolysis process [16]. As the char was oxidised, the production of additional CO and CO_2 resulted in additional mass loss and energy generation. As a result, a lower incident heat flux was required to obtain the same overall MLR. This demonstrated that char oxidation had an effect on the interpretation of the pyrolysis process as the char oxidation is likely to drive more pyrolysis [17,18].

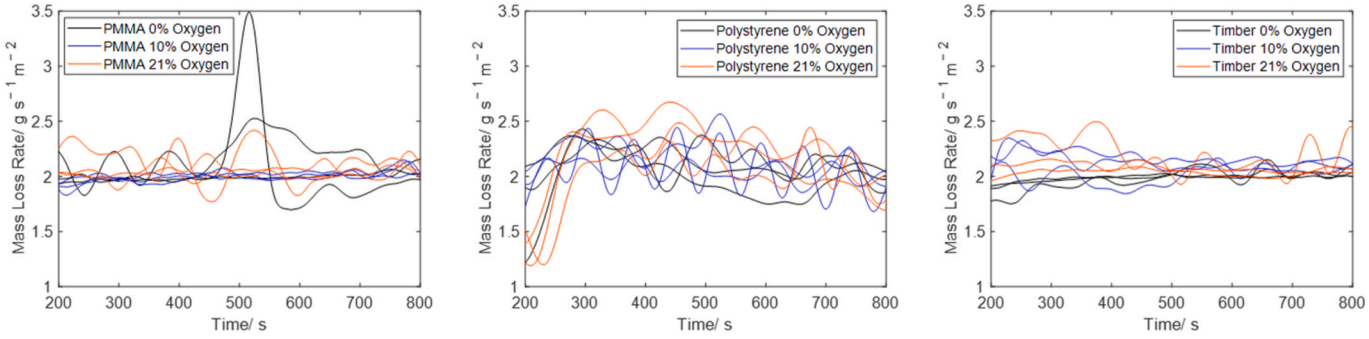

Fig. 3. The smoothed (Gaussian filter, 80 periods) mass loss rates observed for each of the three materials (PMMA, polystyrene and timber) under each of the three oxygen environments (0%, 10% and 21%). Differing material properties resulted in differing responses to the PID controller.

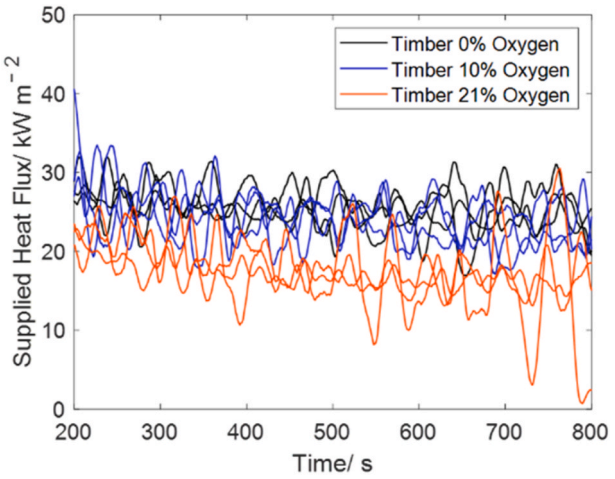

Fig. 4. The heat flux supplied by the FPA during each of the timber runs to achieve a steady state mass loss rate (2 g s^{-1}). The data has been smoothed (Gaussian filter, 20 periods).

3.2. Pyrolysis products

3.2.1. GC-MS speciation

The GC-MS analysis of condensed effluent led to a TIC being obtained for each run. Each peak within the TIC had a mass spectrum recorded, enabling speciation via database matching. Any species with a match greater than 40% has been included at the top of each TIC shown in Figs. 5–7 alongside the relevant retention time (RT).

Utilising external standards alongside the calculated peak areas from the TICs, the peaks representing MMA, styrene and 2-methoxyphenol generated by PMMA, polystyrene and timber could be quantified. The MMA and styrene monomers featured prominently in the effluent for PMMA and polystyrene, respectively, while a simple aromatic phenol was selected to represent timber effluent. Fig. 8 shows the average concentrations of these species obtained from the condensed effluent for each the PMMA, polystyrene and timber runs.

3.2.2. GC-MS yields

As the established MLR was constant, relative to slight fluctuations, throughout each run, the GC-MS data could be assumed to reflect the average composition of the effluent generated over the entirety of the run. As such, any quantified values could be averaged out over the course of an experimental run, facilitating an alternative means of calculating yields.

This GC-MS data was quantified via calibration against responses from known reference compounds. Pure samples (≥99%) of MMA, styrene and 2-methoxyphenol were diluted in DCM to form five different solutions with concentrations ranging from 0.01 to 0.25 mol dm^{-3}. The resultant calibration curves enabled peak areas to be used to calculate product yields.

Once a peak on the TIC, Figs. 5–7, had been selected, its identity was confirmed through the analysis of the MS fragmentation pattern. Upon identification, the peak area was integrated and subsequently converted into a concentration based on calibration with the reference compounds. Equation (2) was used to convert the calculated concentration into a density.

$$\rho\ (g\ dm^{-3}) = C\ (mol\ dm^{-3}) \times M_r\ (g\ mol^{-1}) \tag{2}$$

This density was converted into a mass through multiplication by the added volume of DCM (0.325 dm^3). Equation (3) summarises this step, showing how the masses were obtained.

$$Mass\ (g) = \rho\ (g\ dm^{-3}) \times V\ (dm^3) \tag{3}$$

This obtained mass was divided by the total sample mass loss over the course of a run during the timeframe that the condenser sampling line was switched on (600 s), enabling the calculation of a yield (g g^{-1}). Equation (4) summarises this calculation, facilitating the generation of comparable yields.

$$Yield\ (g\ g^{-1}) = \frac{Mass\ (g)}{Sample\ Mass\ Loss\ (g)} \tag{4}$$

3.2.3. FT-IR speciation

When reviewing the FT-IR sample spectrum obtained from the PMMA runs shown in Fig. 9, three dominant bands, 1152 cm^{-1}, 1355 cm^{-1} and 1750 cm^{-1}, were observed.

Assigning some of the other absorption bands in Fig. 9 to typical alkyl and carbonyl vibrational modes, suggested that the unknown compound or compounds were species with a degree of unsaturation, likely to contain an ester linkage. Despite the complex mixture, the obtained spectra were similar to spectra generated during the synthesis of the polymers, with a close resemblance to the MMA spectrum [19,20]. It was plausible to suggest that this signal had arisen from the MMA monomer or possibly a similar oligomer. This was confirmed through the analysis of the GC-MS data. A prominent peak eluting after ~4.9 min on the TIC shown in Fig. 5, had ions present at 101, 69 and 41 *m/z*; corresponding to the fragmentation pattern and molecular mass of the monomer MMA [20]. This speciation reinforced the analysis of the FT-IR signal, suggesting that the main product was indeed MMA. Additionally, the TIC revealed the identity of many secondary products, including dimethyl 2-methyl-5-methyleneadipate (RT 17.4 in Fig. 5). This species has been shown to form during the polymerisation of MMA, further cementing the MMA peak assignment [21].

Many of the species identified via GC-MS had similar functional groups to MMA and as such would be expected to contribute towards the signal recorded by the FT-IR. The GC-MS confirmed that on average the main pyrolysis product, MMA, accounted for 99.1% of the species extracted from the effluent. This value could subsequently be used to

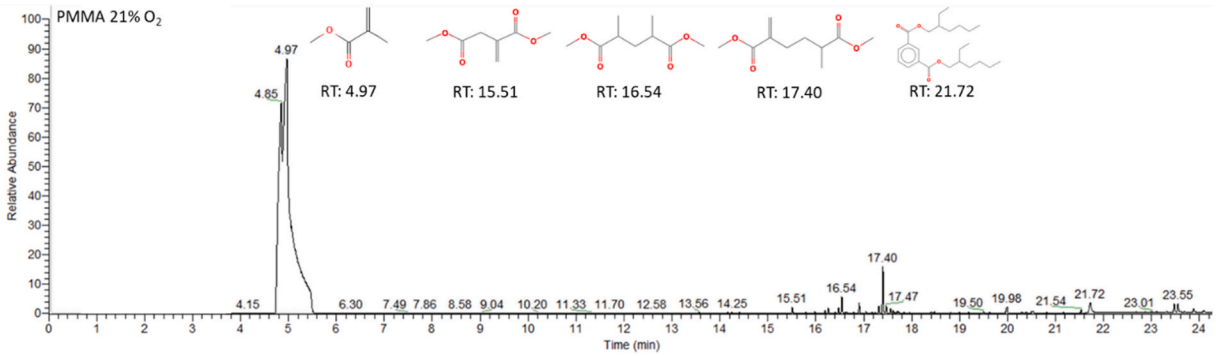

Fig. 5. The total ion chromatogram (TIC) obtained for the pyrolysis of PMMA under 21% O_2. The dominant peak eluting at 4.97 min was identified as MMA.

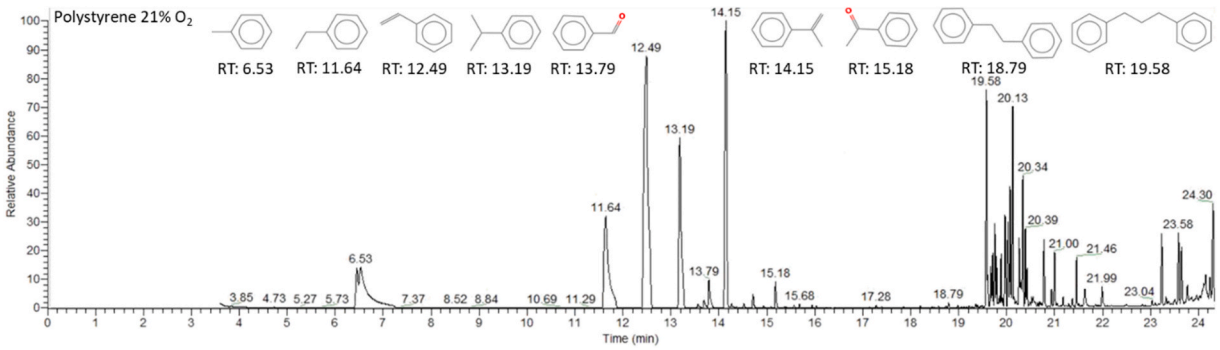

Fig. 6. The total ion chromatogram (TIC) obtained for the pyrolysis of polystyrene under 21% O_2. The peaks eluting at 12.49 and 14.15 min were identified as styrene and methylstyrene.

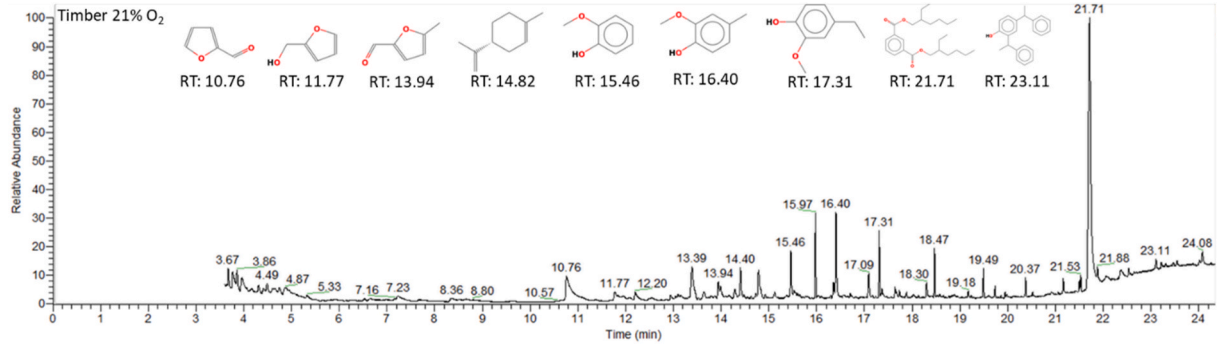

Fig. 7. The total ion chromatogram (TIC) obtained for the pyrolysis of timber under 21% O_2. Many of the identified species were aromatic or heteroaromatic with a particular focus on furans.

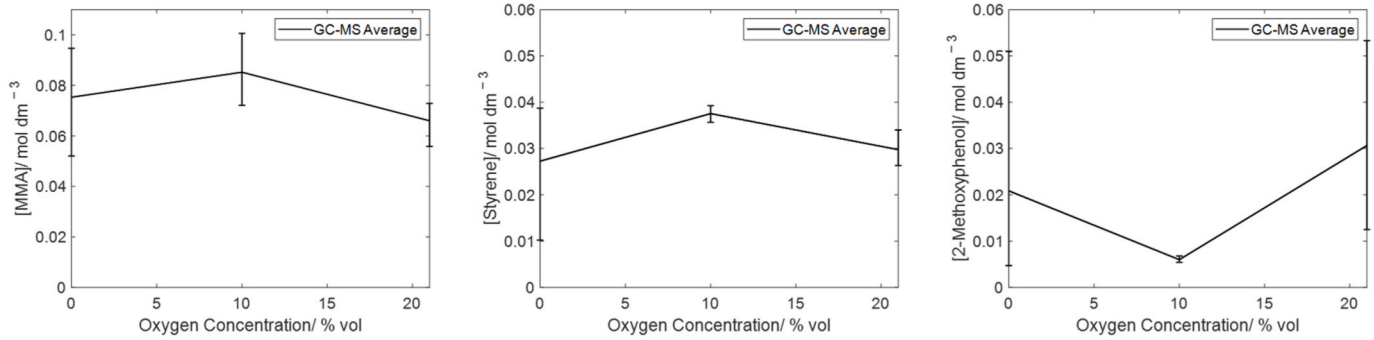

Fig. 8. The average concentrations of MMA, styrene and 2-methoxyphenol recorded via GC-MS, obtained during the pyrolysis of PMMA, polystyrene and timber under three different oxygen environments (0%, 10% and 21% O_2).

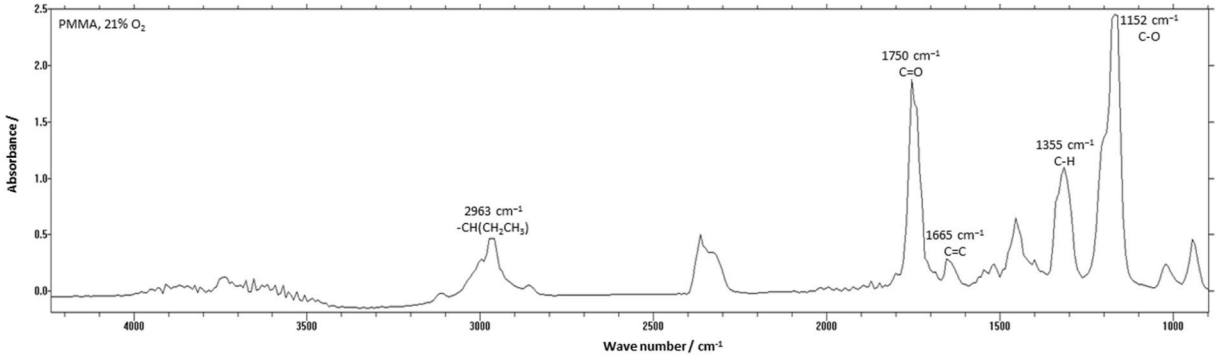

Fig. 9. An FT-IR spectrum obtained during the controlled pyrolysis of PMMA. Prominent bands have been allocated to alkyl, carbonyl and alkene stretching and bending modes.

adjust the yields recorded by the FT-IR.

3.2.4. FT-IR yields

The combination of the constant MLR afforded by the experimental setup with the close-to real time analysis by the FT-IR enabled the species being emitted to be directly related to the pyrolysis process. To enable useful comparisons of the species being generated during these experimental runs, the data required presenting in the form of yields (g g^{-1}).

During each experiment only the analytical tools situated at the end of the heated sampling lines were able to identify species that were not CO, CO_2 or O_2. As the GC-MS data was based upon the condensed effluent summed over the entirety of a run, only the FT-IR data enabled near real-time changes to be tracked. The FT-IR data was recorded in parts per million (ppm), with the relationship summarised by Equation (5).

$$1\ ppm = \frac{1\ \mu mol\ (gas)}{1\ mol\ (air)} \tag{5}$$

It was assumed that the relatively small gaseous species sampled by the FT-IR were unlikely to interact and as such could be assumed to behave as ideal gases. Rearranging the ideal gas law, Equation (6), enabled Equation (7), for molar volume (V_m) to be formed.

$$P\ (Pa) \times V\ (m^3) = n\ (mol) \times R\ (J\ K^{-1}mol^{-1}) \times T\ (K) \tag{6}$$

$$V_m\ (m^3\ mol^{-1}) = \frac{V\ (m^3)}{n(mol)} = \frac{R\ (J\ K^{-1}mol^{-1}) \times T\ (K)}{P\ (Pa)} \tag{7}$$

To obtain the concentration of a species being monitored, ppm values needed to be converted into masses. A density term (ρ) was introduced to describe the relationship between the mass and volume of a gas. Equation (8) described this density term, while Equation (9) showed the relationship between mass and molar mass (M_r).

$$\rho\ (g\ m^{-3}) = \frac{m\ (g)}{V\ (m^3)} \tag{8}$$

$$m\ (g) = n\ (mol) \times M_r\ (g\ mol^{-1}) \tag{9}$$

The substitution of Equations (6) and (9) into Equation (8) generated Equation (10).

$$\rho\ (g\ m^{-3}) = \frac{n\ (mol) \times M_r\ (g\ mol^{-1}) \times P\ (Pa)}{n\ (mol) \times R\ (J\ K^{-1}mol^{-1}) \times T\ (K)} = \frac{M_r\ (g\ mol^{-1}) \times P\ (Pa)}{R\ (J\ K^{-1}mol^{-1}) \times T\ (K)} \tag{10}$$

Equation (7) was substituted into Equation (10) to form Equation (11). At this point the dimensionless ppm reading was converted into a decimal, before being added into Equation (11) to form Equation (12); which enabled the calculation of the density of a species of interest.

$$\rho\ (g\ m^{-3}) = \frac{M_r\ (g\ mol^{-1})}{V_m\ (m^3\ mol^{-1})} \tag{11}$$

$$\rho\ (g\ m^{-3}) = \frac{ppm\ (decimalised) \times M_r\ (g\ mol^{-1})}{V_m\ (m^3\ mol^{-1})} \tag{12}$$

Having calculated the density of the species of interest via Equation (12), it became necessary to calculate the flowrate of air through the experimental setup. Equation (13) detailed the calculation of this flowrate, while Equation (14) enabled the mass flow for the species of interest to be obtained via the combination of these equations.

$$Flow\ Rate\ (m^3\ s^{-1}) = 100\ L\ min^{-1} = \frac{100\ L}{60\ s} = 1.67 \times 10^{-3}\ m^3\ s^{-1} \tag{13}$$

$$Mass\ Flow\ (g\ s^{-1}) = \rho\ (g\ m^{-3}) \times Flow\ Rate\ (m^3\ s^{-1}) \tag{14}$$

Finally, to enable the mass flow rate data to be comparable, the data had to be linked to the rate of material decomposition. Through the division of the average mass loss rate (MLR), theoretically constant at a steady state, a yield could be obtained. This calculation is outlined in Equation (15), accounting for the area of the sample. An example of the average values obtained for MMA across the PMMA runs is included in Table 2.

$$Yield\ (g\ g^{-1}) = \frac{Mass\ Flow\ (g\ s^{-1})}{Average\ MLR\ (g\ s^{-1}m^{-2}) \times Sample\ Area(m^2)} \tag{15}$$

3.3. Improving speciation: The combined use of GC-MS and FT-IR

Each of the deployed analytical techniques utilised in this study had their own merits and drawbacks. The advanced speciation afforded by the GC-MS was limited by the lack of a temporal reading. While the near real-time measurements enabled by the FT-IR failed to distinguish signals arising from similar species. Combining the different techniques reduced their individual limitations, enabling a greater understanding of pyrolysis.

As Fig. 6 shows, during the pyrolysis of polystyrene the GC-MS identified seven different mono-substituted aromatic species with either a methyl or ethyl chain present, including styrene. For the same run, the FT-IR managed to detect both methylbenzene and ethylbenzene, however it was not calibrated to detect the monomer styrene. Consulting the FT-IR spectra, an example is shown in Fig. 10, the characteristic absorption bands for styrene were present including the CC stretch at ~1680 cm^{-1} [22]. However, as the majority of these bands corresponded to aromatic stretching and bending modes, the molecule could only be confirmed to contain an aromatic ring, thus preventing full speciation.

When IR reference spectra for the seven aromatic species detected by the GC-MS during the pyrolysis of polystyrene were overlaid, overlapping bands were present in three distinct regions, ~3000 cm^{-1}, denoting an aromatic C–H stretch, ~1500 cm^{-1}, indicative of aromatic C–C stretching and ~750 cm^{-1}, corresponding to aliphatic C–H bending. The degree of overlap in these regions prevented the FT-IR from distinguishing between these similar species within the effluent.

To mitigate for the limited speciation offered by the FT-IR, yields were adjusted based on the ratios obtained via GC-MS. Continuing with the polystyrene example, the FT-IR readings for the styrene related species, methylbenzene and ethylbenzene, were summed to represent the total signal being produced by mono-substituted aromatic compounds. This value was split based on the GC-MS peak ratios obtained for the five mono-substituted aromatic hydrocarbons. The percentage by area for styrene, averaging at 48.8%, from the GC-MS peaks was used to 'correct' the FT-IR readings, which enabled the styrene yield to be estimated.

A similar adjustment was conducted for the MMA readings, averaging at 99.1%, obtained during the pyrolysis of PMMA. It is likely that the dimers detected via the GC-MS contributed, although minimally, to the total MMA measurement. Fig. 11 shows the adjusted yields obtained for MMA, styrene and 2-methoxyphenol when the GC-MS was combined with the FT-IR readings.

During the pyrolysis of timber, FT-IR analysis failed to detect 2-methoxyphenol or a similar aromatic ether. As such, an adjusted FT-IR yield could not be presented for 2-methoxyphenol. As the GC-MS data appeared to underestimate the yield of MMA, it suggested that the GC-MS yield of 2-methoxyphenol alone was inadequate to obtain a complete picture of the effluent.

The FT-IR analysis of the timber effluent did reveal the identities of species that had boiling points lower than 195 K. Methane yields obtained during the pyrolysis of timber tended to be raised under oxidative conditions. Fig. 12 displays the near real-time yields of MMA, ethylbenzene and methane obtained from the pyrolysis of PMMA, PS and timber respectively.

Table 2
Calculating a yield for MMA based on the average reading recorded by the FT-IR analyser.

Average values for MMA	O_2/%								
	0	0	0	10	10	10	21	21	21
ρ/g m^{-3}	8.93	12.2	9.27	9.77	10.3	9.76	12.3	12.1	10.5
Mass Flow $\times$ 10^{-2}/g s^{-1}	1.49	2.03	1.55	1.63	1.72	1.63	2.06	2.02	1.76
Yield/g g^{-1}	0.71	0.97	0.74	0.78	0.82	0.78	0.98	0.96	0.84

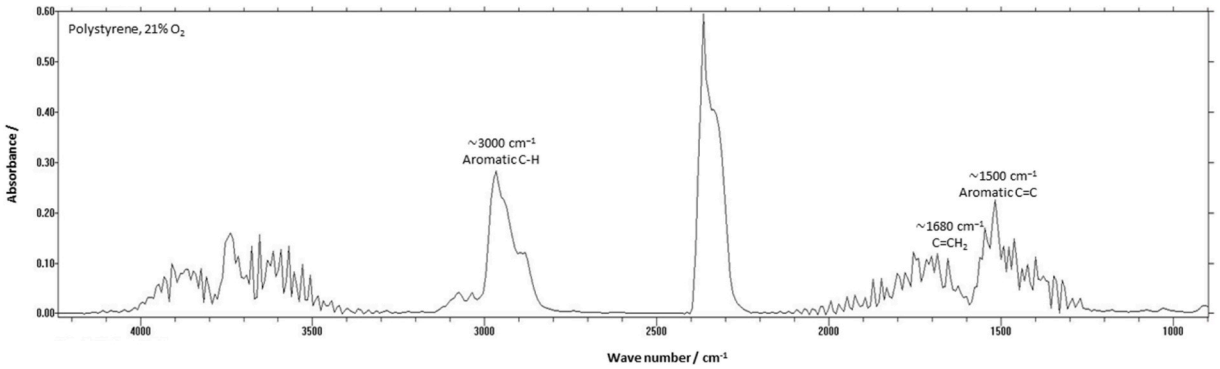

Fig. 10. An FT-IR spectrum obtained during the controlled pyrolysis of polystyrene. Absorption bands have been allocated to aromatic stretching and bending modes. The band at ~1680 cm^{-1} could indicate an alkene C=C stretch or may be a continuation of the aromatic stretching region.

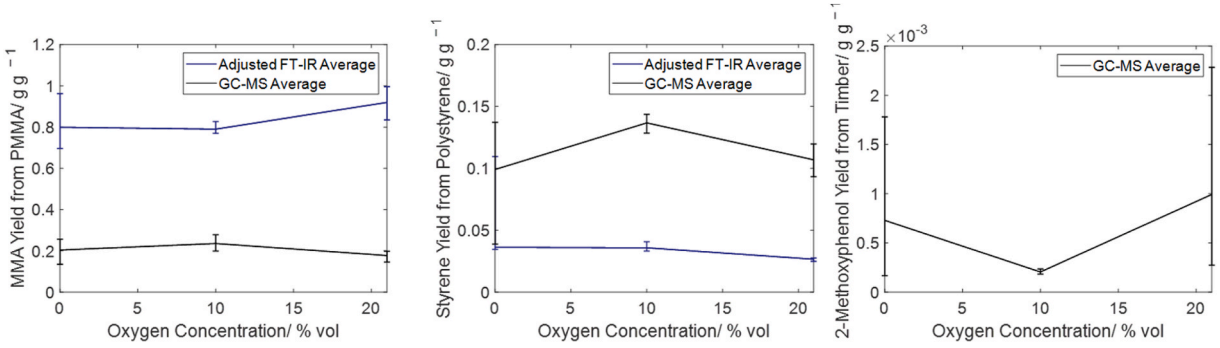

Fig. 11. The GC-MS yields of MMA (left), styrene (centre) and 2-methoxyphenol (right) compared to the corresponding adjusted FT-IR yields obtained during the pyrolysis of PMMA, polystyrene and timber.

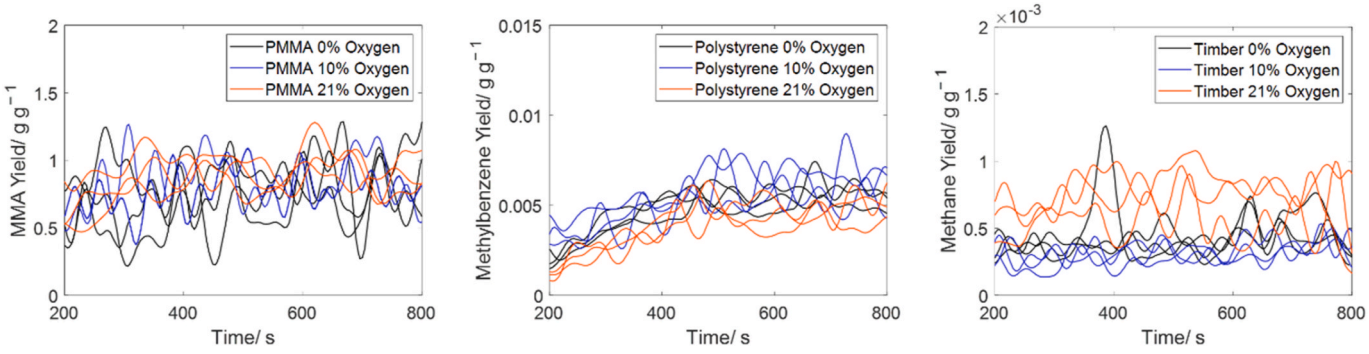

Fig. 12. The smoothed (Gaussian filter, 15 periods) MMA, methylbenzene and methane yields obtained from the FT-IR cell during pyrolysis of PMMA, PS and timber under differing oxidative conditions.

The increased methane levels generated under oxidative conditions suggested that a high temperature process was occurring. It is plausible to propose that the increased temperature afforded by the charring of the timber, confirmed utilising Fig. 4, enabled alternative pyrolysis processes to occur. Further investigation into this process is required, however it is clear that the proposed method facilitated the determination of different pyrolysis pathways.

Styrene and methylbenzene are both mono-substituted aromatic rings, differing in mass by one carbon atom. In the absence of an FT-IR styrene signal, methylbenzene was selected to represent the aromatic species obtained during the pyrolysis of polystyrene. Oxidative environments appeared to hinder methylbenzene production, with yields

increasing and only stabilising once the polystyrene had completely melted. As styrene was a large component of the pyrolysis effluent identified by GC-MS, it was plausible to suggest that styrene would follow a similar relationship to the recorded methylbenzene trend, reflecting the literature [8]. Further work alongside styrene reference spectra would be required to verify these insights.

The obtained MMA yields occasionally peaked above 1 g g^{-1}, suggesting experimental error. This error is likely to have arisen from the FT-IR signal allocation with other non-condensed species potentially influencing the signal. This result identifies room for method development, perhaps utilising cooler refrigerants (e.g. liquid nitrogen) to enhance the insight into pyrolysis and hence the adjustment process. However, the yields indicate that on average MMA comprised 84% of the effluent, mirroring values obtained in literature, thus highlighting the potential of the proposed methodology [23].

4. Concluding remarks

The calculated yields illustrated in Fig. 11 suggested that during pyrolysis the monomer MMA (0.84 g g^{-1}) was the dominant pyrolysis product generated by PMMA. These yields mirrored values recorded in comparative literature for MMA, where yields of 93.5% by mass have been reported [23]. The FT-IR instrument was not calibrated to detect the monomer styrene, however styrene was identified as a main product of the effluent by GC-MS shown by Fig. 6. Given the similarities between the functional groups and thus the observed FT-IR bands between styrene, ethylbenzene and methylbenzene, these species were summed to represent the total signal being produced by mono-substituted aromatic compounds. The calculated styrene yield (0.03 g g^{-1}) was an order of magnitude lower than that of comparative literature, 55.9% by mass, suggesting that the FT-IR measurements required complementary analyses. A GC-MS ratio of 48.8% styrene by area did however correlate with literature, highlighting the importance of combining analytical techniques, and thus the practicality of the proposed methodology [24].

The notable uncertainty observed in the monomer yields suggested that oxygen did not have a significant impact on the pyrolysis of PMMA and polystyrene. Adjusted FT-IR yields based on GC-MS ratios enabled near real-time tracking of species within the effluent. Comments are made on the reported yields for a range of species in relation to the imposed environment, however, a greater number of replicates would be required to confidently comment on the stability of these species in the presence of oxygen.

The most notable observation in the presence of oxygen lay with the charring solid, timber. Under oxidative conditions a lower heat flux, ~25 kW m^{-2}, was delivered to the sample in order to sustain the same MLR, 2 g s^{-1}, as the inert runs. This lower heat flux suggested that char oxidation was occurring alongside pyrolysis, thus contributing to the mass loss. These oxidative processes are likely to have contributed to differences observed in the collected effluent, however natural variation within the polymer could also explain the fluctuations. As such, no notable difference in the type of species being generated during solely the pyrolysis of timber could be identified.

The direct link between sample mass loss and effluent analysis afforded by the proposed methodology has facilitated insights into the pyrolysis processes. This methodology has potential to improve understanding of the pyrolysis process by measurement of real time species yields for a range of products and materials.

Declaration of competing interest

The authors declare that they have no known competing financial interests or personal relationships that could have appeared to influence the work reported in this paper.

Data availability

Data will be made available on request.

References

[1] J. Gong, L. Yang, A review on flaming ignition of solid combustibles: pyrolysis kinetics, experimental methods and modelling, Fire Technol. (2022), https://doi.org/10.1007/s10694-022-01339-7.

[2] C. Huggett, B.C. Levin, Toxicity of the pyrolysis and combustion products of poly (vinyl chlorides): a literature assessment, Fire Mater. 11 (1987), https://doi.org/10.1002/fam.810110303.

[3] C. Fourneau, C. Delvosalle, H. Breulet, S. Brohez, Characterization of highly under-ventilated fires using the cone calorimeter, Fire Mater. 40 (2016) 434–444, https://doi.org/10.1002/FAM.2298.

[4] A. Basch, M. Lewin, The influence of fine structure on the pyrolysis of cellulose. I. Vacuum pyrolysis, J. Polym. Sci. Polym. Chem. Ed. 11 (1973) 3071–3093, https://doi.org/10.1002/POL.1973.170111204.

[5] J.D. Peterson, S. Vyazovkin, C.A. Wight, Kinetic study of stabilizing effect of oxygen on thermal degradation of poly(methyl methacrylate), J. Phys. Chem. B 103 (1999) 8087–8092, https://doi.org/10.1021/JP991582D.

[6] T. Hirata, T. Kashiwagi, J.E. Brown, Thermal and oxidative degradation of poly (methyl methacrylate): weight loss, Macromolecules 18 (1985) 1410–1418, https://doi.org/10.1021/ma00149a010.

[7] A. Witkowski, A.A. Stec, T.R. Hull, Thermal decomposition of polymeric materials, in: SFPE Handbook of Fire Protection Engineering, fifth ed., 2016, pp. 167–254, https://doi.org/10.1007/978-1-4939-2565-0_7.

[8] J.D. Peterson, S. Vyazovkin, C.A. Wight, Kinetics of the thermal and thermo-oxidative degradation of polystyrene, polyethylene and poly(propylene), Macromol. Chem. Phys. 202 (2001) 775–784, https://doi.org/10.1002/1521-3935.

[9] J.M. Challinor, Characterisation of wood by pyrolysis derivatisation—gas chromatography/mass spectrometry, J. Anal. Appl. Pyrolysis 35 (1995) 93–107, https://doi.org/10.1016/0165-2370(95)00903-R.

[10] T. Fateh, F. Richard, T. Rogaume, P. Joseph, Experimental and modelling studies on the kinetics and mechanisms of thermal degradation of polymethyl methacrylate in nitrogen and air, J. Anal. Appl. Pyrolysis 120 (2016) 423–433, https://doi.org/10.1016/J.JAAP.2016.06.014.

[11] A.A. Stec, T.R. Hull, K. Lebek, Characterisation of the steady state tube furnace (ISO TS 19700) for fire toxicity assessment, Polym. Degrad. Stabil. 93 (2008) 2058–2065, https://doi.org/10.1016/J.POLYMDEGRADSTAB.2008.02.020.

[12] ASTM Committee, E2058 Standard Test Methods for Measurement of Material Flammability Using a Fire Propagation Apparatus (FPA), 2019, https://doi.org/10.1520/E2058-19. Technical Report.

[13] S. Santamaria Garcia, Ignition of Solids Exposed to Transient Irradiation, 2021, https://doi.org/10.7488/ERA/1708.

[14] B. Beauregards, Improving the Beginner's PID, 2011. http://brettbeauregard.com/blog/2011/04/improving-the-beginners-pid-introduction/. (Accessed 21 November 2022).

[15] N. Boonmee, J.G. Quintiere, Glowing and flaming autoignition of wood, Proc. Combust. Inst. 29 (2002) 289–296, https://doi.org/10.1016/S1540-7489(02)80039-6.

[16] M.J. Spearpoint, J.G. Quintiere, Predicting the burning of wood using an integral model, Combust. Flame 123 (2000) 308–325, https://doi.org/10.1016/S0010-2180(00)00162-0.

[17] D. Morrisset, R.M. Hadden, A.I. Bartlett, A. Law, R. Emberley, Time dependent contribution of char oxidation and flame heat feedback on the mass loss rate of timber, Fire Saf. J. 120 (2021), 103058, https://doi.org/10.1016/J.FIRESAF.2020.103058.

[18] C.E. Macleod, A. Law, R.M. Hadden, Quantifying the heat release from char oxidation in timber, Fire Saf. J. 138 (2023), 103793, https://doi.org/10.1016/j.firesaf.2023.103793.

[19] O. Yllmaz, Ç.K. Özkan, C.N. Yllmaz, A. Yorgancloğlu, H. Özgünay, H.A. Karavana, Synthesis and characterization of functional acrylic copolymers via RAFT mini-emulsion polymerization, AIP Conf. Proc. 1918 (2017), 20006, https://doi.org/10.1063/1.5018501/720588.

[20] Y. Ding, W. Zhang, X. Zhang, D. Han, W. Liu, J. Jia, Pyrolysis and combustion behavior study of PMMA waste from micro-scale to bench-scale experiments, Fuel 319 (2022), 123717, https://doi.org/10.1016/J.FUEL.2022.123717.

[21] M. Stickler, G. Meyerhoff, Die thermische polymerisation von methylmethacrylat, 2. Bildung des ungesättigten dimeren, Makromol. Chem. 181 (1980) 131–147, https://doi.org/10.1002/MACP.1980.021810113.

[22] V. Hermán, H. Takacs, F. Duclairoir, O. Renault, J.H. Tortai, B. Viala, Core double–shell cobalt/graphene/polystyrene magnetic nanocomposites synthesized by in situ sonochemical polymerization, RSC Adv. 5 (2015) 51371–51381, https://doi.org/10.1039/C5RA06847A.

[23] R. Chen, M. Xu, Kinetic and volatile products study of micron-sized PMMA waste pyrolysis using thermogravimetry and Fourier transform infrared analysis, Waste Manag. 113 (2020) 51–61, https://doi.org/10.1016/J.WASMAN.2020.05.039.

[24] A. Zayoud, H. Dao Thi, M. Kusenberg, A. Eschenbacher, U. Kresovic, N. Alderweireldt, M. Djokic, K.M. Van Geem, Pyrolysis of end-of-life polystyrene in a pilot-scale reactor: maximizing styrene production, Waste Manag. 139 (2022) 85–95, https://doi.org/10.1016/J.WASMAN.2021.12.018.